Journal of Cerebral Blood Flow & Metabolism (2013) 33, 996–999

www.jcbfm.com

BRIEF COMMUNICATION

In vivo NADH fluorescence imaging indicates effect of aquaporin-4 deletion on oxygen microdistribution in cortical spreading depression

Alexander S Thrane[1,2,3,5], Takahiro Takano[1,5], Vinita Rangroo Thrane[1,2,3,5], Fushun Wang[1], Weiguo Peng[1], Ole Petter Ottersen[2], Maiken Nedergaard[1] and Erlend A Nagelhus[1,2,3,4]

Using *in vivo* two-photon imaging, we show that mice deficient in aquaporin-4 (AQP4) display increased fluorescence of nicotinamide adenine dinucleotide (NADH) when subjected to cortical spreading depression. The increased NADH signal, a proxy of tissue hypoxia, was restricted to microwatershed areas remote from the vasculature. *Aqp4* deletion had no effects on the hyperemia response, but slowed $[K^+]_o$ recovery. These observations suggest that K^+ uptake is suppressed in *Aqp4*$^{-/-}$ mice as a consequence of decreased oxygen delivery to tissue located furthest away from the vascular source of oxygen, although increased oxygen consumption may also contribute to our observations.

Journal of Cerebral Blood Flow & Metabolism (2013) **33,** 996–999; doi:10.1038/jcbfm.2013.63; published online 24 April 2013

Keywords: AQP4; astrocytes; glia; NADH; metabolic

INTRODUCTION

Aquaporin-4 (AQP4) is the principal brain water channel and is concentrated in astrocytic endfoot membranes at the brain–blood and brain–liquor interfaces.[1] It is surprising that our understanding of the physiologic roles of AQP4 has evolved so slowly given its abundance in brain. Although AQP4 is engaged in interstitial fluid dynamics under physiologic conditions,[2,3] several lines of work show that animals must be subjected to severe stress for a clear *Aqp4*$^{-/-}$ phenotype to become apparent. The role of AQP4 in mediating water exchange across the blood–brain interface was, for instance, initially demonstrated in models of brain edema that entail pronounced osmotic stress.[4]

Here we used cortical spreading depression (CSD) as a model of severe metabolic stress to resolve whether oxygenation of brain neuropil depends on the presence of AQP4. Drawing on experience from studies of brain edema, we hypothesized that severe stress would be needed to disclose a link between AQP4 expression and tissue oxygenation.[4] Cortical spreading depression is a slowly spreading wave of depressed neuronal activity associated with a massive buildup of extracellular concentration of K^+ ions ($[K^+]_o$), thought to occur during migraine headaches. The recovery of $[K^+]_o$ involves several mechanisms, including inward rectifying K^+-channels, (Na^+)–K^+–Cl^- cotransporters, and the Na^+, K^+-ATPase.[5–7]

Two-photon imaging of nicotinamide adenine dinucleotide (NADH) fluorescence can be used to provide high-resolution maps of tissue redox state *in vivo*. Increased NADH signal is a sensitive nonlinear proxy of tissue hypoxia.[8] Our analysis shows that *Aqp4* deletion leads to a more pronounced oxygen deficit in microwatershed areas and a protracted $[K^+]_o$ recovery. The most parsimonious explanation of these observations is that removal of AQP4 reduces oxygen supply and hence slows K^+ re-uptake.

MATERIALS AND METHODS

Mouse Preparation

Aqp4$^{-/-}$ and *Aqp4*$^{+/+}$ mice of either sex were generated as previously described and anesthetized using intraperitoneal urethane (1 g/kg) and α-chloralose (50 mg/kg).[9] The mice were prepared for *in vivo* two-photon imaging as previously described.[7] Cortical spreading depression was evoked by either pressure injecting 1 M KCl through a micropipette or surface application of 1 M KCl (5 μl) through a small secondary craniotomy. Fixation of mice, preparation of tissue slices, and immunohistochemistry were performed as described previously.[9] All animal experiments were conducted in accordance with the ARRIVE guidelines and approved by the Animal Care and Use Committee of the University of Rochester.

In Vivo Recordings

A Mai Tai HP (Spectra Physics, Irvine, CA, USA) attached to a confocal scanning system (FV300, Olympus, Melville, NY, USA) and an upright microscope (IX51W) with an $\times 20$ objective (0.95 NA, Olympus) was used. We performed combined imaging of NADH and intravascular fluorescein isothiocyanate-dextran (2000 kDa, 5%, intravenous).[7] Nicotinamide adenine dinucleotide was excited at 740 nm and emission was detected using a 460 nm filter (50 nm bandwidth), while fluorescein isothiocyanate-dextran emission was detected using a 515 nm filter (50 nm bandwidth). The images were taken every 3 s at 50–150 μm depth. Images were filtered and converted to percent changes from baseline using ImageJ software (NIH, Bethesda, MD, USA) as described previously.[7] The NADH fluorescence changes during CSD reveal a characteristic biphasic response.[7] This response has a complex geometry, and perivascular 'cylinders' of low NADH signal can be seen whose size depends both on their

[1]Division of Glial Disease and Therapeutics, Center for Translational Neuromedicine, University of Rochester Medical Center, Rochester, New York, USA; [2]Centre for Molecular Biology and Neuroscience, Letten Centre, Institute of Basic Medical Sciences, University of Oslo, Oslo, Norway; [3]Centre for Molecular Medicine Norway, Nordic EMBL Partnership, University of Oslo, Oslo, Norway and [4]Department of Neurology, Oslo University Hospital, Oslo, Norway. Correspondence: Dr M Nedergaard, Division of Glial Disease and Therapeutics, Center for Translational Neuromedicine, University of Rochester Medical Center, 601 Elmwood Avenue, Rochester, New York 14642, USA.
E-mail: nedergaard@urmc.rochester.edu
This work was supported by the US National Institutes of Health (NS075177 and NS078304 to M.N.), Research Council of Norway (NevroNor, and FUGE grants), Letten Foundation, and Fulbright Foundation.
[5]These authors contributed equally to this work.
Received 18 December 2012; revised 20 February 2013; accepted 18 March 2013; published online 24 April 2013

vascular oxygen content and on their diameter.[8] We therefore calculated the change in signal intensity of individual pixels normalized to values in a baseline image ($\Delta F/F_0$), before the onset of CSD. By convention, the regions where pixel values became more negative ($\Delta F/F_0 < 0$) and positive ($\Delta F/F_0 > 0$) during the CSD wave were defined as 'dip' and 'overshoot', respectively.[7] Direct current potentials and $[K^+]_o$ were recorded using glass microelectrodes and tissue pO_2 (tpO_2) was measured using a Clark-type polarographic oxygen microelectrode (OX-4, Unisense, Aarhus, Denmark) as outlined before.[7,10] Cerebral blood flow was assessed using a fiberoptic laser Doppler probe (PF5010, Perimed, Stockholm, Sweden) and connected to an infrared laser Doppler flowmeter. All signals were digitized (Digidata 1332A, Molecular Devices, Sunnyvale, CA, USA) and analyzed (pClamp 10.2, Molecular Devices, Sunnyvale, CA, USA).

RESULTS

Deletion of *Aqp4* Increases Microwatershed NADH Fluorescence During Cortical Spreading Depression

We measured tissue NADH fluorescence, cerebral blood flow, tissue oxygen tension (tpO_2), local field potentials, and $[K^+]_o$ in living wild-type and *Aqp4*$^{-/-}$ mice after induction of CSD (Figure 1A). Immunofluorescence confirmed high perivascular AQP4 expression in wild-type mice and confirmed the efficacy of the gene knockout strategy (Figure 1B). The total and perivascular dip NADH responses in *Aqp4*$^{-/-}$ animals did not differ from that in wild type during CSD (Figures 1C and 1D). However, the overshoot region of the NADH response was greater in the *Aqp4*$^{-/-}$ animals than in wild types almost from the onset

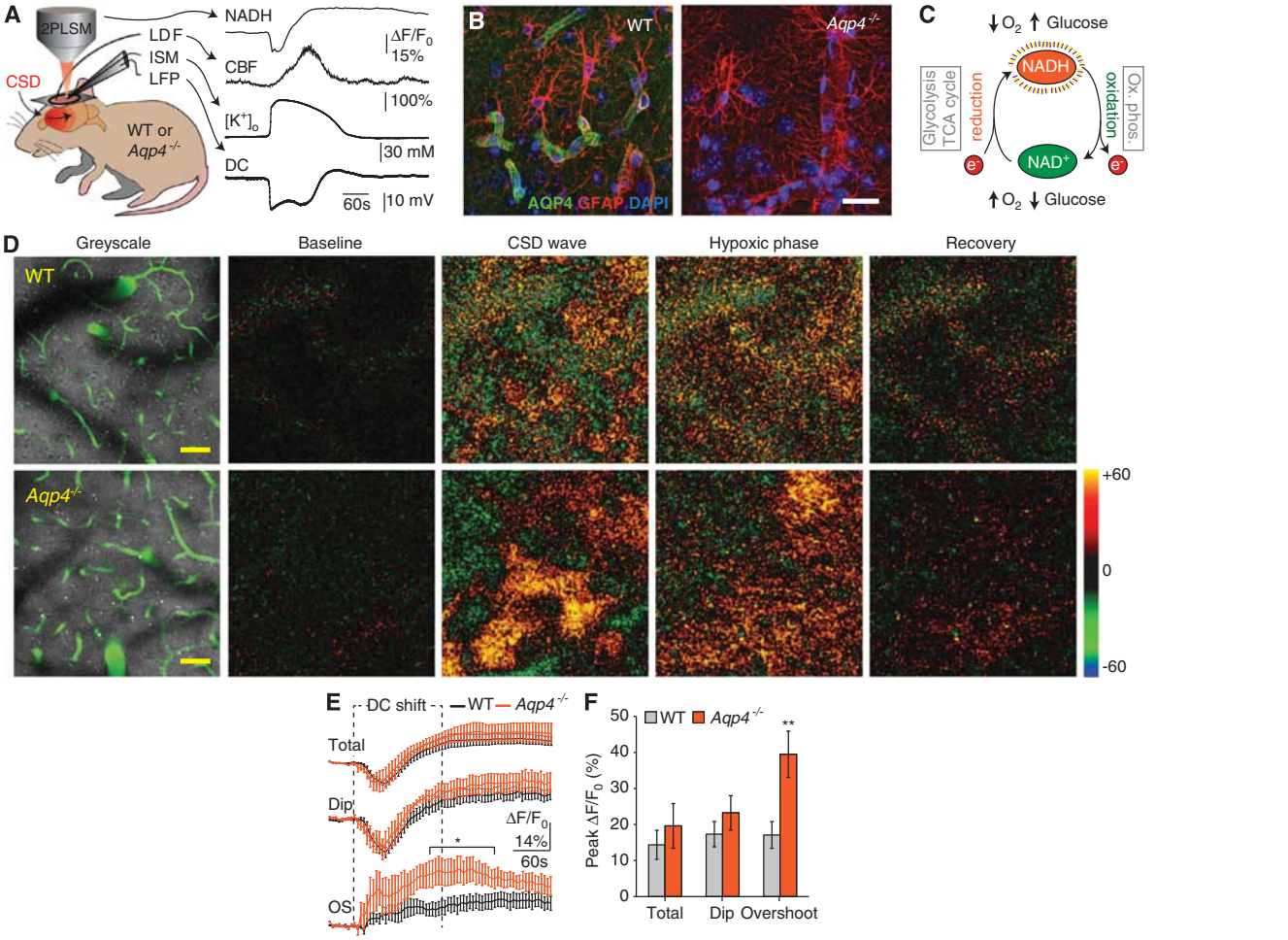

Figure 1. Deletion of aquaporin-4 (*Aqp4*) increased nicotinamide adenine dinucleotide (NADH) fluorescence in microwatershed areas during cortical spreading depression (CSD). (**A**) Experimental setup. After induction of CSD in living *Aqp4*$^{-/-}$ and wild-type (WT) mice, we measured changes in NADH fluorescence with 2PLSM, cerebral blood flow with laser Doppler flowmetry, extracellular concentration of K^+ ($[K^+]_o$) with K^+-ion-sensitive microelectrodes, direct current potential, and tissue partial pressure of oxygen (tpO2) (not illustrated). (**B**) Immunofluorescence micrographs from WT and *Aqp4*$^{-/-}$ mice illustrating AQP4 expression in cerebral cortex. AQP4 (green), GFAP (red), and DAPI (blue). (**C**) Endogenous NAD^+ and its reduced counterpart NADH are key coenzymes in glycolysis, the citric acid cycle, and the mitochondrial respiratory chain. Since only NADH is fluorescent (and not NAD^+), two-photon NADH imaging offers maps of tissue redox state that can be used as a proxy of tissue oxygenation. (**D**) *Left*: NADH fluorescence images of cerebral cortex in WT (75 μm depth) and *Aqp4*$^{-/-}$ (105 μm depth) mice. Green denotes fluorescein isothiocyanate-dextran labeled blood vessels. Nicotinamide adenine dinucleotide fluorescence is largely uniform, except where NADH is made less visible by the presence of large pial vessels at the surface of the brain. *Right*: Representative false color images of change in NADH fluorescence ($\Delta F/F_0$) from baseline intensity, during the early (CSD wave) and late phase of CSD (hypoxic phase), and after recovery. In the early phase of CSD, when the DC potential dropped, cortical tissue showed a complex pattern of NADH decrease (dip, shown in green) and increase (overshoot, shown in red/orange). At a later stage, when DC potential had normalized, all regions showed increased NADH fluorescence (hypoxic phase), before gradually returning to baseline level. Scale bar represents 50 μm. (**E**) Running average traces ($\Delta F/F_0$) for the biphasic NADH response during CSD, showing whole field ('total'), dip and overshoot in WT and *Aqp4*$^{-/-}$ mice. Duration of DC shift is indicated. $^*P < 0.05$, $n =$ five animals in each group, unpaired *t* test. (**F**) Bar graph representing the peak change in NADH fluorescence in WT and *Aqp4*$^{-/-}$ mice. $P = 0.394$ (total), 0.329 (dip), and 0.00762 (overshoot), $n =$ five animals in each group, unpaired *t* test. Data are shown as mean ± s.e.m.

of CSD, and became significantly higher ~2 minutes after the onset (total neuropil: wild type 14.36 ± 4.02% vs. *Aqp4*$^{-/-}$ 19.61 ± 6.21%; dip: wild type 17.33 ± 3.43% vs. *Aqp4*$^{-/-}$ 23.23 ± 4.78%; overshoot: wild type 17.09 ± 3.71% vs. *Aqp4*$^{-/-}$ 39.48 ± 6.43%, all peak values, $P < 0.05$ for 145 to 250 seconds post CSD onset) (Figures 1E and 1F). The rising phase of NADH fluorescence overshoot lasted 187.50 ± 36.54 seconds in wild-type and 133.33 ± 49.09 seconds in *Aqp4*$^{-/-}$ animals, and was not significantly different (data not shown). Thus, our data suggest that *Aqp4* deletion selectively impairs tissue oxygenation in areas furthest away from the vasculature.

Deletion of *Aqp4* Does not Influence Hyperemia and Vascular Oxygen Supply in Cortical Spreading Depression

Cerebral blood flow is critical for maintaining adequate tissue oxygenation. Owing to the strong AQP4 expression around blood vessels, we tested whether *Aqp4* deletion influenced the vascular response to CSD. Neither the amplitude nor the duration of the hyperemia phase differed between wild-type and *Aqp4*$^{-/-}$ animals (peak: wild type 164.50 ± 4.57% vs. *Aqp4*$^{-/-}$ 162.57 ± 7.54%; duration: wild type 174.50 ± 11.56 seconds vs. *Aqp4*$^{-/-}$ 178.06 ± 6.09 seconds) (Figures 2A–2C). Additionally, *Aqp4* deletion did not affect overall tissue oxygen supply, which we assessed using oxygen-sensitive microelectrodes that integrate tpO_2 from an ~268–524 μm^3 volume encompassing both NADH dip and overshoot regions (baseline: wild type 38.60 ± 3.14mm Hg vs. *Aqp4*$^{-/-}$ 45.98 ± 4.88 mm Hg; CSD: wild type 9.14 ± 2.05mm Hg vs. *Aqp4*$^{-/-}$ 11.53 ± 3.03 mm Hg; Figure 2D).[7] The kinetics of these tpO_2 recordings was not significantly different (Figures 2E and 2F) (ΔtpO_2: wild type −29.46 ± 4.98 vs. *Aqp4*$^{-/-}$ −34.45 ± 3.13; declining slope: wild type −2.79 ± 1.22 mm Hg/second vs. *Aqp4*$^{-/-}$ −3.44 ± 0.74 mm Hg/second; recovery slope: wild type +0.67 ± 0.38 mm Hg/second vs. *Aqp4*$^{-/-}$ +0.58 ± 0.12 mm Hg/second). Finally, when we used tpO_2 and blood flow recordings to approximate the cerebral metabolic rate of oxygen ($\Delta CMRO_2$), this was not significantly different between the two genotypes during CSD (wild type 281.50 ± 21.62 μmol/100 g per minute vs. *Aqp4*$^{-/-}$ 292.50 ± 23.40 μmol/100 g per minute,

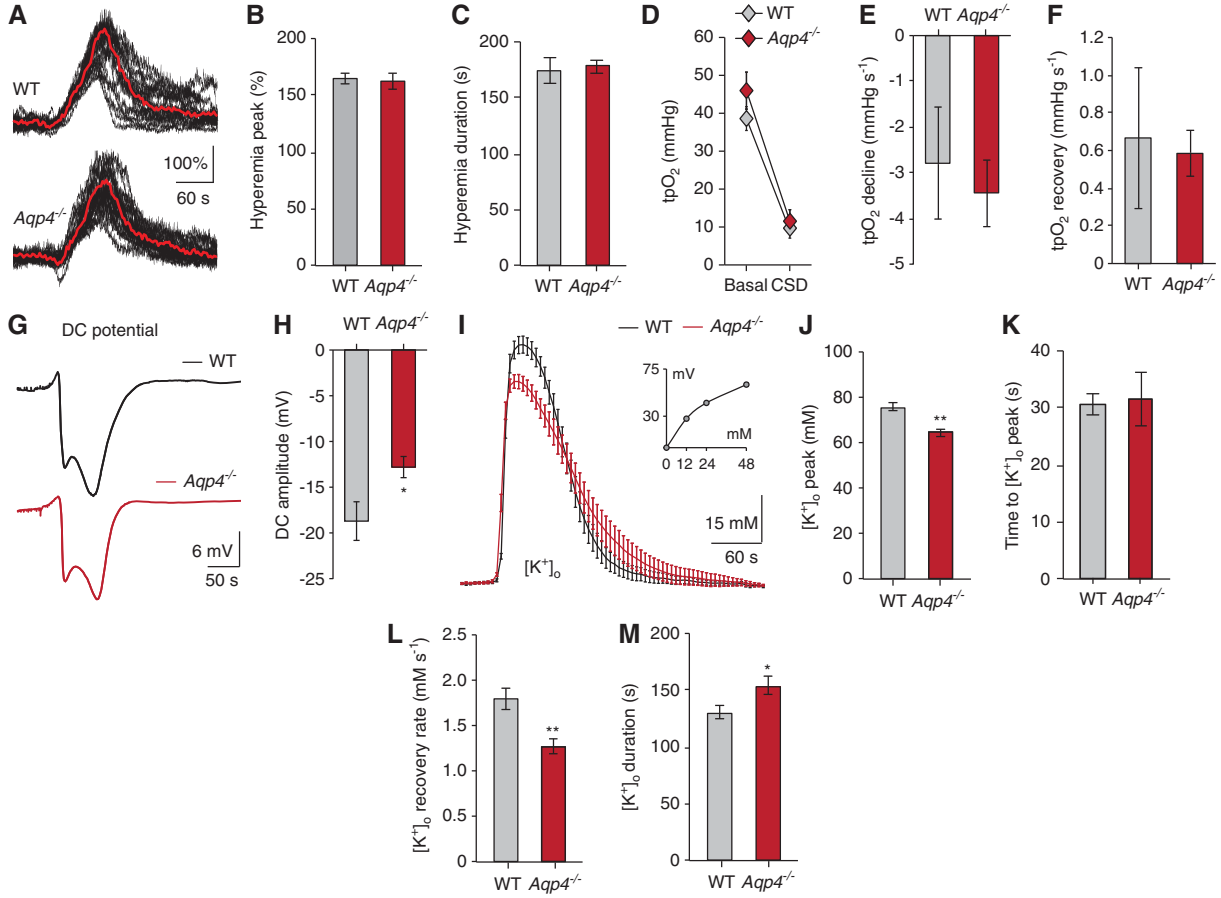

Figure 2. Deletion of aquaporin-4 (*Aqp4*) did not affect vascular oxygen supply but delayed extracellular K^+ clearance in cortical spreading depression (CSD). (**A**) Representative laser Doppler recordings (black) and a running average of these recordings (red) demonstrating the hyperemic response during CSD in *Aqp4*$^{-/-}$ and WT mice. (**B, C**) Bar graphs summarizing the effect of *Aqp4* deletion on peak amplitude and duration of the CSD hyperemic response. $P = 0.876$ (peak), 0.794 (duration), $n = 22$ wild-type (WT) and 41 *Aqp4*$^{-/-}$ stimulations from seven WT and 12 *Aqp4*$^{-/-}$ animals, unpaired *t* test. (**D**) Line graph showing mean cortical tpO_2 before (basal) and during CSD in WT and *Aqp4*$^{-/-}$ mice, measured using oxygen-sensitive microelectrodes. $P = 0.264$ (base), 0.555 (trough), $n = 6$ WT and eight *Aqp4*$^{-/-}$ animals, unpaired *t* test. (**E, F**) Bar graphs showing mean cortical tpO_2 slope decline and recovery. $P = 0.641$ (decline), $P = 0.818$ (recovery), $n = 6$ WT and eight *Aqp4*$^{-/-}$ animals, unpaired *t* test. (**G, H**) Representative traces and bar graphs summarizing the effects of *Aqp4* deletion on amplitude of the DC-shift. $^*P = 0.0223$, $n = 6$ (WT) and eight (*Aqp4*$^{-/-}$) animals, unpaired *t* test. (**I**) Running averages of extracellular concentration of K^+ ($[K^+]_o$) during CSD for WT (black) and *Aqp4*$^{-/-}$ mice (red), acquired using K^+-ion-sensitive-microelectrodes. Inset: K^+-ISM calibration curve. $n = 7$ (WT) and 12 (*Aqp4*$^{-/-}$). (**J-M**) Bar graphs summarizing the effect of *Aqp4* deletion on peak $[K^+]_o$, time to peak, $[K^+]_o$ recovery rate, and duration of $[K^+]_o$ elevation in CSD. $[K^+]_o$ peak is reduced and $[K^+]_o$ recovery is delayed in *Aqp4*$^{-/-}$ mice. $^*P = 0.0459$ (duration), $^{**}P < 0.001$ (peak and recovery rate), $P = 0.855$ (time to peak), $n = 22$ (WT) and 41 (*Aqp4*$^{-/-}$) CSD responses from seven WT and 12 (*Aqp4*$^{-/-}$) animals, unpaired *t* test. Data are shown as mean ± s.e.m.

data not shown). However, this calculation uses equivalent coefficients for oxygen diffusion through brain in both genotypes, which may be an incorrect assumption if AQP4 alters gas diffusion. Taken together, we found no evidence that deleting *Aqp4* altered hyperemia or overall oxygen supply during CSD.

Deletion of *Aqp4* Delays $[K^+]_o$ Recovery in Cortical Spreading Depression

The amplitude of the direct current potential shift, which is dependent on $[K^+]_o$, was significantly lower in *Aqp4*$^{-/-}$ than in wild-type mice (amplitude: wild type -18.71 ± 2.11 mV vs. *Aqp4*$^{-/-}$ -12.80 ± 1.16 mV) (Figures 2G and 2H). In line with these data and the finding that *Aqp4* deletion increases basal extracelluar space volume,[11] the amplitude of the $[K^+]_o$ increase was significantly lower in *Aqp4*$^{-/-}$ animals (amplitude: wild type 75.54 ± 1.86 mM vs. *Aqp4*$^{-/-}$ 64.49 ± 1.73 mM) (Figures 2I and 2J). The rising phase of $[K^+]_o$ in CSD lasted 30.53 ± 1.76 seconds in wild-type and 31.61 ± 4.75 s in *Aqp4*$^{-/-}$ animals, not significantly different (Figure 2K). However, *Aqp4*$^{-/-}$ mice showed a slower $[K^+]_o$ recovery compared with wild types (recovery rate: wild type 1.79 ± 0.12 mM/s vs. *Aqp4*$^{-/-}$ 1.27 ± 0.08 mM/second; duration of $[K^+]_o$ elevation: wild type 130.32 ± 5.42 seconds vs. *Aqp4*$^{-/-}$ 153.86 ± 7.54 seconds) (Figures 2L and M), suggesting that the capacity for $[K^+]_o$ clearance is reduced by *Aqp4* deletion.

DISCUSSION

Our study provides the first line of evidence that AQP4 impacts oxygenation of brain tissue. Using CSD as a model of severe metabolic stress, we show that *Aqp4* deletion increases NADH fluorescence in areas furthest away from cerebral microvessels. NADH fluorescence is a sensitive indicator of tissue hypoxia with a p_{50} of 3.4 mm Hg,[8] and our data thus demonstrate that *Aqp4* deletion enhances the already critical microwatershed hypoxia seen in CSD.[7] Measurements with laser Doppler flowmetry show that this impaired oxygenation was not due to inadequate blood supply, as *Aqp4*$^{-/-}$ and wild-type mice had a comparable hyperemia response. Moreover, oxygen-sensitive microelectrodes showed that the observed NADH changes did not reflect overall differences in tissue oxygenation, but were spatially restricted to microwatershed regions.

The observed increase of microwatershed hypoxia in *Aqp4*$^{-/-}$ mice can be explained by either enhanced oxygen consumption or reduced oxygen diffusion. *Aqp4* deletion has previously been shown to impair $[K^+]_o$ clearance during CSD, seizures, and neuronal stimulation.[2,3,5,6,12] AQP4 can impact $[K^+]_o$ clearance in several ways, including regulating extracellular space volume, dissipating osmotic gradients arising from ion transport, and enhancing interstitial bulk flow.[2,3,6,12] *Aqp4* deletion might therefore increase microwatershed hypoxia by making perivascular $[K^+]_o$ homeostasis less efficient and consume excess oxygen. However, this hypothesis would imply that *Aqp4*$^{-/-}$ mice have a larger perivascular NADH signal dip and a higher overall oxygen uptake, neither of which we found in our study. Additionally, the hypothesis would predict that $[K^+]_o$ increases in the *Aqp4*$^{-/-}$ mice prior to the observed NADH changes, whereas our data indicate the opposite.

The alternative hypothesis entails *Aqp4* deletion impairing oxygen diffusion across perivascular endfoot membranes. Experimental analyses in oocytes and modeling studies have suggested that AQP4 might serve as a gas channel.[13,14] Wang and Tajkhorshid[13]suggested that the central pore of the AQP4 tetramer could conduct NO and O_2. However, the membrane permeability for gasses likely varies significantly depending on the type of gas studied (O_2, CO_2, NO), lipid composition of the membrane (e.g. endfoot vs. oocyte), and macromolecular organization of transmembrane proteins (e.g. AQP4 tetramers). Aquaporin-facilitated gas transport is therefore an unresolved topic, where several studies have presented evidence for and against the hypothesis.[13–15] If oxygen diffusion were rate limiting in our study, we would hypothesize that microwatershed hypoxia would be increased and involve a larger area, which the NADH imaging supports. We might also expect that inadequate oxygenation - through compromised Na^+-K^+-ATPase activity - precedes and potentially causes the slowed $[K^+]_o$ clearance seen in *Aqp4*$^{-/-}$ mice, and our data show a tendency towards this. Finally, NADH is an indirect and nonlinear indicator of tissue hypoxia that can be influenced by factors unrelated to oxygenation (e.g. cell swelling, hypoglycemia). As we were unable to detect an overall difference in tissue oxygenation using microelectrodes, our data therefore do not directly show that mitochondrial oxygen uptake is inadequate or rate limiting in the *Aqp4*$^{-/-}$ mice.

In conclusion, our data suggest that *Aqp4* deletion in CSD impairs the oxygenation of areas remote from brain microvessels. These observations are consistent with the hypothesis that AQP4 facilitates oxygen diffusion, but due to methodological limitations, we cannot conclusively differentiate this from the alternative explanation that *Aqp4* deletion increases metabolic demand. Our study thus provides the first evidence to suggest that AQP4 is involved in facilitating oxygen diffusion *in vivo*.

DISCLOSURE/CONFLICT OF INTEREST

The authors declare no conflict of interest.

REFERENCES

1 Nielsen S, Nagelhus EA, Amiry-Moghaddam M, Bourque C, Agre P, Ottersen OP. Specialized membrane domains for water transport in glial cells: high-resolution immunogold cytochemistry of aquaporin-4 in rat brain. *J Neurosci* 1997; **17**: 171–180.
2 Iliff JJ, Wang M, Liao Y, Plogg BA, Peng W, Gundersen GA *et al.* A paravascular pathway facilitates CSF flow through the brain parenchyma and the clearance of interstitial solutes, including amyloid beta. *Sci Transl Med* 2012; **4**: 147ra11.
3 Strohschein S, Huttmann K, Gabriel S, Binder DK, Heinemann U, Steinhauser C. Impact of aquaporin-4 channels on K+ buffering and gap junction coupling in the hippocampus. *Glia* 2011; **59**: 973–980.
4 Manley GT, Fujimura M, Ma T, Noshita N, Filiz F, Bollen AW *et al.* Aquaporin-4 deletion in mice reduces brain edema after acute water intoxication and ischemic stroke. *Nat Med* 2000; **6**: 159–163.
5 Mazel T, Richter F, Vargova L, Sykova E. Changes in extracellular space volume and geometry induced by cortical spreading depression in immature and adult rats. *Physiol Res* 2002; **51**(Suppl 1): S85–S93.
6 Padmawar P, Yao X, Bloch O, Manley GT, Verkman AS. K+ waves in brain cortex visualized using a long-wavelength K+-sensing fluorescent indicator. *Nat Methods* 2005; **2**: 825–827.
7 Takano T, Tian GF, Peng W, Lou N, Lovatt D, Hansen AJ *et al.* Cortical spreading depression causes and coincides with tissue hypoxia. *Nat Neurosci* 2007; **10**: 754–762.
8 Kasischke KA, Lambert EM, Panepento B, Sun A, Gelbard HA, Burgess RW *et al.* Two-photon NADH imaging exposes boundaries of oxygen diffusion in cortical vascular supply regions. *J Cereb Blood Flow Metab* 2011; **31**: 68–81.
9 Thrane AS, Rappold PM, Takumi F, Ottersen OP, Nedergaard M, Nagelhus EA. Critical role of aquaporin-4 (AQP4) in astrocytic Ca2+ signaling events elicited by cerebral edema. *Proc Natl Acad Sci USA* 2010; **108**: 846–851.
10 Wang F, Xu Q, Wang W, Takano T, Nedergaard M. Bergmann glia modulate cerebellar Purkinje cell bistability via Ca2+-dependent K+ uptake. *Proc Natl Acad Sci USA* 2012; **109**: 7911–7916.
11 Yao X, Hrabetova S, Nicholson C, Manley GT. Aquaporin-4-deficient mice have increased extracellular space without tortuosity change. *J Neurosci* 2008; **28**: 5460–5464.
12 Binder DK, Yao X, Zador Z, Sick TJ, Verkman AS, Manley GT. Increased seizure duration and slowed potassium kinetics in mice lacking aquaporin-4 water channels. *Glia* 2006; **53**: 631–636.
13 Wang Y, Tajkhorshid E. Nitric oxide conduction by the brain aquaporin AQP4. *Proteins* 2010; **78**: 661–670.
14 Musa-Aziz R, Chen LM, Pelletier MF, Boron WF. Relative CO2/NH3 selectivities of AQP1, AQP4, AQP5, AmtB, and RhAG. *Proc Natl Acad Sci USA* 2009; **106**: 5406–5411.
15 Fang X, Yang B, Matthay MA, Verkman AS. Evidence against aquaporin-1-dependent CO2 permeability in lung and kidney. *J Physiol* 2002; **542**: 63–69.